Self-Isolated Raman Lasing with a Chiral Dielectric Metasurface

Jefferson Dixon,[1] Mark Lawrence,[2] David R. Barton III,[2] and Jennifer Dionne[2]
[1]Department of Mechanical Engineering, Stanford University, Stanford, California 94305, USA
[2]Department of Materials Science and Engineering, Stanford University, Stanford, California 94305, USA

(Received 25 March 2020; accepted 13 January 2021; published 23 March 2021)

The light sources that power photonic networks are small and scalable, but they also require the incorporation of optical isolators that allow light to pass in one direction only, protecting the light source from damaging backreflections. Unfortunately, the size and complex integration of optical isolators makes small-scale and densely integrated photonic networks infeasible. Here, we overcome this limitation by designing a single device that operates both as a coherent light source and as its own optical isolator. Our design relies on high-quality-factor dielectric metasurfaces that exhibit intrinsic chirality. By carefully manipulating the geometry of the constituent silicon metaatoms, we design three-dimensionally chiral modes that act as optical spin-dependent filters. Using spin-polarized Raman scattering together with our chiral metacavity, we demonstrate Raman lasing in the forward direction, while the lasing action is suppressed by over an order of magnitude for reflected light. Our high-Q chiral metasurface design presents a new approach toward compactly isolating integrated light sources by directly tailoring the emission properties of the light source itself.

DOI: 10.1103/PhysRevLett.126.123201

Integrated photonics promises the broadband, high-density, and high-speed interconnectivity necessary for advanced telecommunication networks and high-performance signal processing. Coherent light sources are critical components of such photonic systems, and these devices should be compact, efficient, and preferably compatible with mature CMOS fabrication technologies [1]. While considerable progress has been made in developing integrated light sources [2–5], the resonant nature of these light sources dictates that these photonic systems are sensitive to small perturbations caused by unwanted reflections and defects [6]. An optical isolator solves this issue by serving as a one-way valve for light, in which light is blocked in one direction but allowed to pass in the opposite direction, protecting the laser from backreflections, reducing unwanted interference and allowing for greater interconnectivity [7]. Isolation is critical to the realization of photonic networks, without which we are limited to low-power sources with sparse interconnection and impractically long optical pathways.

The most common embodiment of optical isolation, a Faraday isolator, relies on a fixed magnetic bias to break reciprocity for a time-reversed pair of modes. However, breaking reciprocity without further modal restriction is not sufficient to define isolation; consequently, a Faraday isolator includes polarization filters to restrict access to modes that would otherwise propagate in the forbidden direction. Unfortunately, the weak interaction of magnetic fields with most materials at optical frequencies makes a Faraday isolator much larger ($>100\ \mu$m) than the integrated light sources we seek to isolate [8].

New nonreciprocal photonic components attempt to overcome this scaling problem by enhancing light-matter interactions through resonant confinement in high quality factor (i.e., high-Q) dielectric structures [9–18]. In recent work, a periodic array of subwavelength nanoantennas (i.e., a metasurface) is used to resonantly confine a circularly polarized optical bias that breaks optical reciprocity [19]. Conveniently, the high-Q confinement of the metasurface cavity can also be used to amplify an optical pump or signal, similar to other periodic dielectric structures that have been used to demonstrate compact, low-threshold lasing [2,3,17]. Analogously to the requirement of polarization filters in a Faraday isolator, the metasurface cavity is nonreciprocal but requires further modal restriction to be isolated.

Here, we present a new approach to isolate integrated light sources by tailoring the modal properties of the lasing cavity itself, specifically using a spin-selective chiral metasurface cavity excited with spin-polarized stimulated Raman scattering. Using full-field electromagnetic simulations, we explore a silicon metasurface composed of notched cylinders resonant in the near infrared. By manipulating the coupling between neighboring cylinders in a dimer unit cell, we achieve an intrinsically chiral optical response with a spin-selective transmittance for orthogonal polarizations of circularly polarized light. To break Lorentz reciprocity explicitly, we excite the metasurface with a spin-polarized Raman pump that mimics the magnetic bias in a Faraday isolator [19]. Consequently, a signal beam at a frequency Stokes-shifted from the Raman pump is only amplified when the signal obeys photon-phonon spin selection rules imposed by the Raman pump in addition to separate spin selection rules

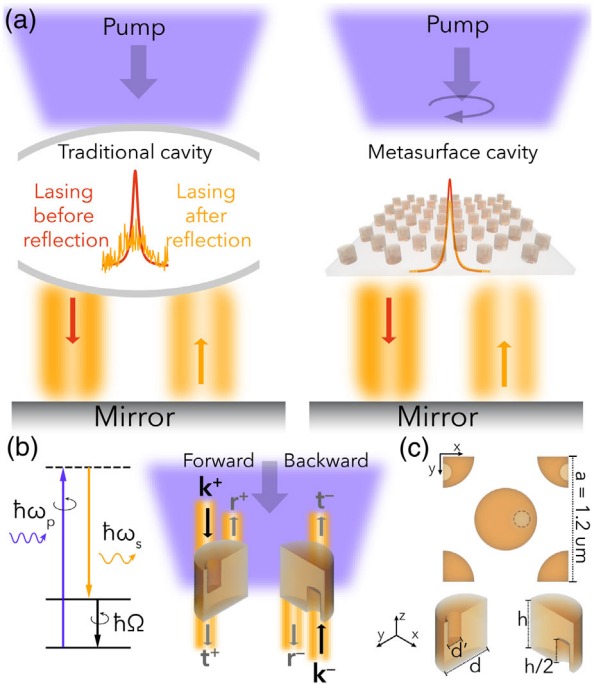

FIG. 1. (a) Schematic of self-isolated metasurface laser. The Raman pump (purple) results in stimulated emission at the Stokes frequency (yellow). Left: In a traditional laser cavity, the original lasing mode (red) is destroyed when reflected light reenters the cavity (yellow). Right: Because of spin-selective modal restriction of the metasurface cavity, the lasing mode remains undisturbed upon reflection. (b) Energy diagram for Raman decay of a pump photon into a Stokes photon and a phonon, with a reference legend defining forward (backward) transmission (reflection). (c) The chiral metasurface, comprised of cylinders in a dimer unit cell arranged in a square lattice with periodicity $a = 1.2\ \mu$m and antisymmetric notches, where $d = 600$ nm, $h = 600$ nm and $d' = 160$ nm.

imposed by the symmetry of the chiral metasurface [Figs. 1(a) and 1(b) [19,20]]. A signal with a given polarization state transmits with amplification in one direction, but its reflection (or time-reversed signal) is suppressed in the metasurface cavity, resulting in a self-isolated lasing mode.

A schematic of the metasurface is shown in Fig. 1(c). The unit cell of the metasurface array is composed of two silicon ($n = 3.45$) cylinders in a square lattice, each 600 nm tall and 600 nm in diameter with a lattice periodicity of 1.2 μm. Both cylinders in the dimer unit cell are modified with the introduction of notches, 160 nm in diameter and 300 nm in depth. In one cylinder, the notch is translated in the y direction, while in the other cylinder, the notch is translated in the x and–z directions. The geometry is necessarily three-dimensionally chiral, as a planar chiral geometry will maintain a symmetric response in the forward and backward directions and therefore cannot act as a filter for the same handedness of light from both directions [21,22]. To the best of our knowledge, intrinsic chirality has not been observed in a subwavelength-nondiffracting dielectric metamaterial system [23–26].

While spin-selective optical properties have been reported in plasmonic (i.e., metallic) metasurfaces, three-dimensional chirality in dielectric metasurfaces requires near-field interactions that are not guaranteed with a geometrically chiral structure. For any material platform, optical chirality is defined by the coupling of electric and magnetic fields along the same direction, as described by the generalized constitutive relations [21],

$$\bar{D} = \varepsilon_0 \bar{\bar{\varepsilon}}\, \bar{E} + \frac{i}{c_0} \bar{\bar{\xi}}\, \bar{H}, \qquad \bar{B} = \frac{i}{c_0} \bar{\bar{\zeta}}\, \bar{E} + \mu_0 \bar{\bar{\mu}}\, \bar{H}. \quad (1)$$

Here, $\bar{\bar{\varepsilon}}$, $\bar{\bar{\mu}}$, $\bar{\bar{\xi}}$, and $\bar{\bar{\zeta}}$ are 2×2 complex-valued matrices representing permittivity, permeability, and coupling of the magnetic (electric) field to electric (magnetic) dipoles, respectively. The coupling terms are more explicitly written for reciprocal media as

$$\bar{\bar{\xi}} = -\bar{\bar{\zeta}}^T = \begin{pmatrix} \xi'_C & \xi'_\Omega \\ \xi''_\Omega & \xi''_C \end{pmatrix}, \quad (2)$$

where the off-diagonal components indicate omega-type bianisotropy and the diagonal components are strictly chiral. Plasmonic structures support effective dipole moments that rely on incident light interacting with free electrons on the surface of the metal, where an electric dipole resonance is easily achieved by orienting a wire along the direction of the incident electric field, and a magnetic dipole resonance is achieved by shaping the wire into a current loop (e.g., a split ring resonator) [27]. Accordingly, the magnetic resonance in plasmonic objects is inherently coupled to the electric resonance from which it is formed, and therefore the magnetic resonance of a plasmonic geometry is already a coupled magnetoelectric mode. In contrast, dielectric structures support both electric and magnetic modes inherently within the volume of the material itself, as described by Mie theory [28], and these modes are decoupled from one another. Engineering chiral modes in dielectric objects therefore requires us to carefully consider how geometric perturbations and symmetry conditions affect coupling of the independent modes.

To achieve a three-dimensionally chiral metasurface, we employ a four-step approach to designing the constituent nanoantennas and unit cell: (i) spectrally overlapping the electric and magnetic modes; (ii) breaking out-of-plane mirror symmetry to couple the overlapped modes; (iii) eliminating rotational symmetry to reorient the direction of the electric mode relative to the magnetic mode; and (iv) breaking the remaining in-plane mirror symmetry to induce a spin-selective response. Alternate approaches also exist for the design of intrinsic chirality in subwavelength dielectric systems [25,29,30]. We first tune the spectral position of the electric and magnetic resonances individually by modifying the diameter and height of the cylinders, respectively [31,32] (Supplemental Material, Sec. I [33]). Then, we introduce a notch into the center of the cylinders that breaks

mirror symmetry out of the plane of the metasurface to couple the electric and magnetic modes.

A key characteristic of this bianisotropic (magnetoelectric) coupling is asymmetry in reflection, which for a lossless material appears in the relative phase of the reflection [34]. This asymmetry cannot be observed in transmission because the phase relationship of the electric and magnetic nearfields remains constant as the wave vector orientation remains constant, while flipping the wave vector direction in reflection also flips the phase relationship of the magnetoelectric coupling. Figure 2(a) plots the transmission through the notched metasurface and the difference in the forward and backward reflected phase.

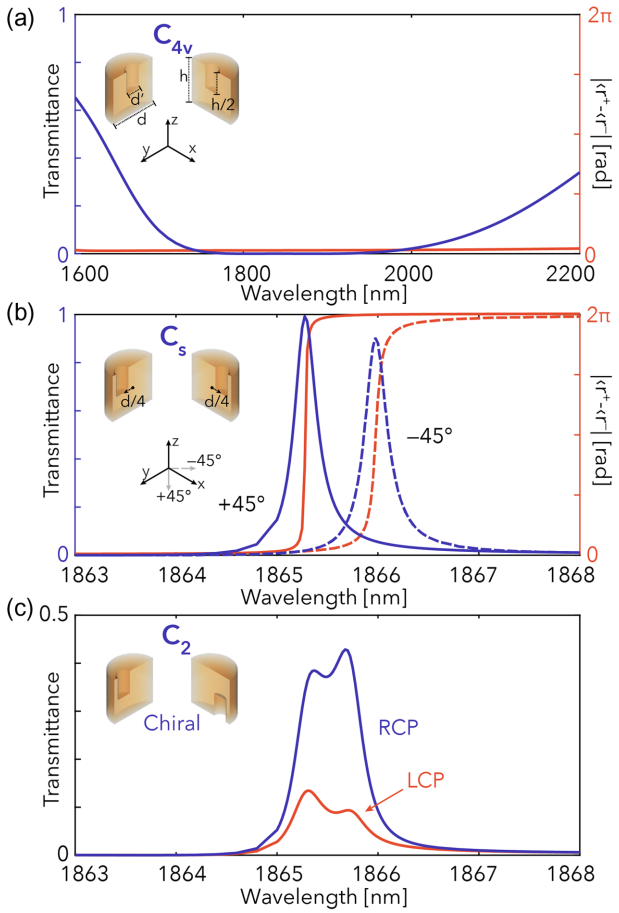

FIG. 2. Transmission (a)–(c) and differential reflected phase to show bianisotropy (a),(b) for the given unit cell geometry and associated point group symmetry (inset), where $d = 600$ nm, $h = 600$ nm, and $d' = 160$ nm. (a) Cylinders notched in the center: Transmission shows low-Q response over which electric and magnetic dipolar modes exist, and the differential reflection reveals weak but nonzero bianisotropy. (b) Translating the notches antisymetrically: Transmission reveals two high-Q resonances corresponding to illumination with $+45°$ and $-45°$ polarization, both of which exhibit strong bianisotropy in the phase of reflection. (c) Inverting every other notch: Differential transmission is observed for illumination for left-handed versus right-handed circularly polarized light, indicating chirality.

The transmission reveals a broad reflective background from the dipolar magnetic and electric modes (1700–2100 nm), and the differential reflected phase reveals a weak but nonzero bianisotropic response ($\xi_\Omega \neq 0$) with $|\angle r^+ - \angle r^-| = 0.03\pi$, where $\angle r^+$ is the phase of reflected light incident from the forward direction [Fig. 1(b)]. Here, the strength of magnetoelectric coupling is limited by the low Q factor associated with such broad magnetic and electric resonances. Regardless of the strength of the response, we now have a symmetry breaking tool to control magnetoelectric coupling and therefore the phase relationship between the electric and magnetic resonances of the metasurface [35,36]. Note, however, that this response remains degenerate for orthogonal polarizations due to the presence of rotational symmetry.

To differentiate orthogonal polarization states, we eliminate rotational symmetry from the lattice by translating the notch in the x direction in one cylinder and symmetrically in the y direction in the neighboring cylinder. This translation reorients the direction of the dipole moments without the further removal of silicon, so as to not disrupt the dipolar characteristic of the modes that occur within the volume. Importantly, this subtle symmetry breaking also increases the Q factor of the metasurface, resulting in a strong bianisotropic response $|\angle r^+ - \angle r^-| = \pi$. Illuminating the metasurface with light polarized along the $\pm 45°$ symmetry axes, two distinct peaks in transmission, with Q's of 7040 and 6980 and are seen for the two polarization states at 1865.3 and 1865.7 nm, respectively [see Fig. 2(b)]. This splitting is characteristic of a dimer unit cell, which exhibits a lower energy symmetric (bonding) mode and a higher energy antisymmetric (antibonding) mode. Here, the mirror symmetry across the $+45°$ axis is the only symmetry remaining in the lattice that prevents a chiral response.

Finally, we shift the notches to the bottom of every other cylinder, leading to a chiral, spin-selective response in transmission. A chiral medium must orient at least some component of the electric and magnetic dipole moments along the same direction [37], which we accomplish by exploiting a coupled dimer unit cell. This configuration allows the electric dipole of one cylinder to couple with the magnetic dipole of its neighbor, resulting in a nonzero ξ_C term in Eq. (2) [38,39]. Consequently, we achieve the chiral optical response shown in Fig. 2(c). On resonance at 1865.5 nm, left- and right-handed circularly polarized (LCP and RCP) light is transmitted with a relative difference of $t_L/t_R = 5$ (Supplemental Material [33], Sec. II). This difference can be enhanced even further [33,40–42], but here we are more limited by polarization conversion between LCP and RCP and not the difference in transmittance between LCP and RCP. The two distinct peaks at 1865.3 and 1865.7 nm in Fig. 2(c) exactly correspond to the two eigenstates produced in Fig. 2(b), which have only changed in direction and not in energy. Importantly, by

relying solely on small notches, the electric field remains concentrated within the silicon (Fig. S2a [33]). While this intrinsically chiral metasurface exhibits asymmetric transmission for a given polarization state, it necessarily remains reciprocal without a time-dependent or nonlinear modification to the constitutive parameters.

The metasurface becomes a self-isolated light source when a circularly polarized pump bias is introduced. In particular, we utilize spin-polarized stimulated Raman scattering (SRS) to explicitly break reciprocity. Pumping a Raman-active crystal with sufficiently intense light results in the spontaneous creation of a phonon, which generates a Stokes-shifted spectral sideband [Fig. 1(b)] [43]. Introducing a second light source at the sideband frequency stimulates this process, resulting in Raman amplification of this second, signal beam [2,20]. This process defines stimulated Raman scattering and Raman lasing. Considering stimulated Raman scattering in a spin-polarized basis, spin selection rules arise for photon-phonon interactions that dictate when stimulated emission occurs. This condition is met in silicon for pump and signal beams of opposite handedness when propagating in the same direction, which we refer to as the forward direction [19,44,45]. While a spin-polarized Raman bias is sufficient to achieve nonreciprocal gain for a time-reversed pair of modes, a signal propagating in the backward direction will still experience gain if the signal is not polarized with the appropriate handedness, as is the case upon reflection of the signal (Fig. S3 [33]). However, in a three-dimensionally chiral metasurface, the modes which correspond to the Raman forbidden polarization are restricted from being excited.

The symmetry of the Raman tensor describes how the phonon mode vibrates spatially in response to the pump electric field [46]. We note that when pumping silicon with circularly polarized light, the pump induces an antisymmetric susceptibility perturbation, in which $\chi_{xy} = -\chi_{yx}$, where χ is the susceptibility modification. This process provides amplification for one circularly polarized mode of a time-reversed pair and consequently breaks reciprocity. The details of the Raman tensor and calculation are described in Sec. III of the Supplemental Material [33] (see also Ref. [19]). Moreover, the local field confinement provided by our high-Q metasurface can greatly reduce the necessary pump power. The existing structure exhibits local field enhancement of $|E|/|E_0| = 74$ at 1865.5 nm and Q's of 4810 (at 1865.3 nm) and 5100 (at 1865.7 nm) while maintaining the rotation of the local electric field (Fig. S2 [33]).

The resulting isolatorlike behavior and nonreciprocal lasing is described in Fig. 3(a). We fix the pump to be LCP and observe transmission (t) and reflection (r) of the signal as we vary the pump power. While the metasurface is designed for intrinsic chirality, the presence of linear birefringence dictates that the polarization basis of the chiral

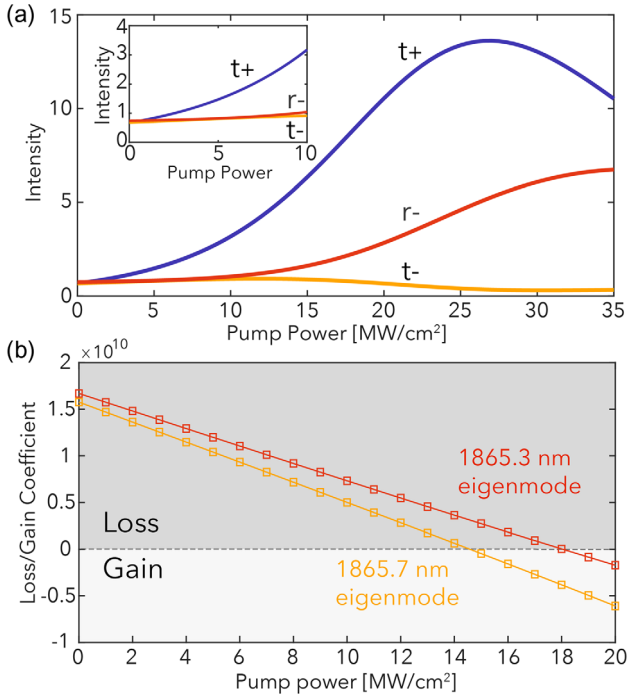

FIG. 3. (a) Transmittance and reflectance of the signal as a function of the pump power with a left-handed circularly polarized pump. Inset: The plot is recreated with a decibel scale. (b) The imaginary component of the complex eigenfrequencies of the chiral metasurface, plotted as a function of the pump power. Red corresponds to the 1865.3 nm eigenmode and yellow corresponds to the 1865.7 nm eigenmode from Fig. 2.

mode is neither entirely circular nor linear. To accommodate the ellipticity of the metasurface eigenmodes, we consider a signal polarized in the basis of the chiral resonance, which we obtain by solving for the eigenvectors of the transmission scattering matrix (Supplemental Material [33], Sec. III i). The signal polarization state by this method is given by its Jones vector $E = [0.9803 + 0i, -0.1822 + 0.0770i]$, which is nearly linearly polarized. For any complete polarization basis, we begin to observe amplification of a forward-propagating signal ($t+$) and suppression of its reflection ($r-$) starting around 2 MW/cm^2 [Fig. 3(a)]. A backward-propagating signal ($t-$) is suppressed and does not experience gain. We consider this system in an entirely circular basis and an entirely linear basis in Sec. IV of the Supplemental Material [33], and we observe amplification of the forward signal and suppression of the backward signal regardless of the signal polarization. Therefore, the dominant and appreciable gain giving rise to lasing only occurs for a signal polarization state and single propagation direction, making our three-dimensionally chiral metasurface a self-isolated laser.

We perform an eigenmode analysis of the metasurface to provide direct evidence of lasing behavior and exemplify the response dependence on the signal frequency. As seen in Fig. 3(b), the metasurface exhibits negative damping

(i.e., gain) at increasing pump powers for both of the chiral eigenmodes, where the zero crossing for the two eigenmodes occurs at approximately 14.5 MW/cm^2 for the eigenmode at 1865.7 nm and 18 MW/cm^2 for the eigenmode at 1865.3 nm. The difference between the transmitted signal and its reflection can be maximized by tuning the signal frequency relative to the two eigenfrequencies of the metasurface, which can also be modified by modifying the metasurface dimensions (Supplemental Material [33], Sec. IV). Generally, we observe that a Raman lasing mode exists in which the lasing cavity (i.e., the chiral metasurface) is self-isolating and the reflection is suppressed, regardless of the signal polarization or signal power.

In summary, we present a submicron lasing cavity with a nonzero chirality parameter and asymmetric permittivity that, together, impose isolation on the lasing mode emitted from that cavity. Here, optical isolation is not considered as an additional photonic component but as a feature built natively into the light source itself. Importantly, we break Lorentz reciprocity with a spin-polarized Raman bias that avoids dynamic reciprocity, which has no lower size limit and can be applied to a wide array of dielectric materials [19]. We present a broad parameter space over which the lasing properties can be optimized, including modifying the chiral resonance by changing the nanoantenna dimensions, tuning the signal frequency relative to the two eigenmodes of the metasurface, and/or modifying the signal polarization. To further reduce the lasing threshold, this platform could capitalize on recent developments in ultrahigh-Q and doubly resonant cavities [47–49]. Beyond subwavelength nonreciprocal and multifunctional integrated light sources, our three-dimensional chiral metasurface could also enable advances in topological photonics and nanophotonic sensing platforms [23,50–54].

We gratefully acknowledge conversations with H. Reddy. Funding was generously provided from the AFOSR under Grant No. FA9550-20-1-0120, as well as from the "Photonics at Thermodynamic Limits" Energy Frontier Research Center funded by the U.S. Department of Energy, Office of Science, Office of Basic Energy Sciences under Award No. DE-SC0019140. J. D. was additionally supported by a Kodak Foundation Fellowship.

Note added.—After the submission of this publication, two recent publications have described the symmetry rules for bound states in the continuum with intrinsic chirality [29,30].

[1] Z. Zhou, B. Yin, and J. Michel, On-chip light sources for silicon photonics, Light **4**, e358 (2015).

[2] H. Rong, R. Jones, A. Liu, O. Cohen, D. Hak, A. Fang, and M. Paniccia, A continuous-wave Raman silicon laser, Nature (London) **433**, 725 (2005).

[3] Y. Takahashi, Y. Inui, M. Chihara, T. Asano, R. Terawaki, and S. Noda, A micrometre-scale Raman silicon laser with a microwatt threshold, Nature (London) **498**, 470 (2013).

[4] Y. D. Kim, Y. Gao, R.-J. Shiue, L. Wang, O. B. Aslan, M.-H. Bae, H. Kim, D. Seo, H.-J. Choi, S. H. Kim, A. Nemilentsau, T. Low, C. Tan, D. K. Efetov, T. Taniguchi, K. Watanabe, K. L. Shepard, T. F. Heinz, D. Englund, and J. Hone, Ultrafast graphene light emitters, Nano Lett. **18**, 934 (2018).

[5] S. Bao, D. Kim, C. Onwukaeme, S. Gupta, K. Saraswat, K. H. Lee, Y. Kim, D. Min, Y. Jung, H. Qiu, H. Wang, E. A. Fitzgerald, C. S. Tan, and D. Nam, Low-threshold optically pumped lasing in highly strained germanium nanowires, Nat. Commun. **8**, 1845 (2017).

[6] Anthony E. Siegman, *Lasers* (University Science Books, Taiwan, 1986).

[7] D. Jalas, A. Petrov, M. Eich, W. Freude, S. Fan, Z. Yu, R. Baets, M. Popović, A. Melloni, J. D. Joannopoulos, M. Vanwolleghem, C. R. Doerr, and H. Renner, What is—and what is not—an optical isolator, Nat. Photonics **7**, 579 (2013).

[8] A. K. Zvezdin and V. A. Kotov, *Modern Magnetooptics and Magnetooptical Materials* (CRC Press, Boca Raton, 1997).

[9] L. Bi, J. Hu, P. Jiang, D. H. Kim, G. F. Dionne, L. C. Kimerling, and C. A. Ross, On-chip optical isolation in monolithically integrated non-reciprocal optical resonators, Nat. Photonics **5**, 758 (2011).

[10] B. Peng, Ş. K. Özdemir, F. Lei, F. Monifi, M. Gianfreda, G. L. Long, S. Fan, F. Nori, C. M. Bender, and L. Yang, Parity–time-symmetric whispering-gallery microcavities, Nat. Phys. **10**, 394 (2014).

[11] M. Lawrence, D. R. Barton, and J. A. Dionne, Nonreciprocal flat optics with silicon metasurfaces, Nano Lett. **18**, 1104 (2018).

[12] Z. Yu and S. Fan, Complete optical isolation created by indirect interband photonic transitions, Nat. Photonics **3**, 91 (2009).

[13] A. M. Mahmoud, A. R. Davoyan, and N. Engheta, All-passive nonreciprocal metastructure, Nat. Commun. **6**, 8359 (2015).

[14] Z. Shen, Y.-L. Zhang, Y. Chen, C.-L. Zou, Y.-F. Xiao, X.-B. Zou, F.-W. Sun, G.-C. Guo, and C.-H. Dong, Experimental realization of optomechanically induced non-reciprocity, Nat. Photonics **10**, 657 (2016).

[15] J. Y. Chin, T. Steinle, T. Wehlus, D. Dregely, T. Weiss, V. I. Belotelov, B. Stritzker, and H. Giessen, Nonreciprocal plasmonics enables giant enhancement of thin-film Faraday rotation, Nat. Commun. **4**, 1599 (2013).

[16] Y. Zhang, Q. Du, C. Wang, T. Fakhrul, S. Liu, L. Deng, D. Huang, P. Pintus, J. Bowers, C. A. Ross, J. Hu, and L. Bi, Monolithic integration of broadband optical isolators for polarization-diverse silicon photonics, Optica **6**, 473 (2019).

[17] A. Kodigala, T. Lepetit, Q. Gu, B. Bahari, Y. Fainman, and B. Kanté, Lasing action from photonic bound states in continuum, Nature (London) **541**, 196 (2017).

[18] M. Lawrence, D. Barton, J. Dixon, J Song, J. van de Groep, M. L. Brongersma, J. Dionne, High quality factor phase gradient metasurfaces, Nat. Nanotechnol. **15**, 956, (2020).

[19] M. Lawrence and J. A. Dionne, Nanoscale nonreciprocity via photon-spin-polarized stimulated Raman scattering, Nat. Commun. **10**, 3297 (2019).

[20] R. W. Boyd, *Nonlinear Optics* (Elsevier, New York, 2003).
[21] I. V. Lindell, A. H. Sihvola, S. A. Tretyakov, and A. J. Viitanen, *Electromagnetic Waves in Chiral and Bi-Isotropic Media* (Artech House Boston, Boston, 1994).
[22] W. Ye, X. Yuan, C. Guo, J. Zhang, B. Yang, and S. Zhang, Large Chiroptical Effects in Planar Chiral Metamaterials, Phys. Rev. Applied **7**, 054003 (2017).
[23] C. Wu, N. Arju, G. Kelp, J. A. Fan, J. Dominguez, E. Gonzales, E. Tutuc, I. Brener, and G. Shvets, Spectrally selective chiral silicon metasurfaces based on infrared Fano resonances, Nat. Commun. **5**, 3892 (2014).
[24] Z. Ma, Y. Li, Y. Li, Y. Gong, S. A. Maier, and M. Hong, All-dielectric planar chiral metasurface with gradient geometric phase, Opt. Express **26**, 6067 (2018).
[25] A. Y. Zhu, W. T. Chen, A. Zaidi, Y.-W. Huang, M. Khorasaninejad, V. Sanjeev, C.-W. Qiu, and F. Capasso, Giant intrinsic chiro-optical activity in planar dielectric nanostructures, Light **7**, 17158 (2018).
[26] M. V. Gorkunov, O. Y. Rogov, A. V. Kondratov, V. V. Artemov, R. V. Gainutdinov, and A. A. Ezhov, Chiral visible light metasurface patterned in monocrystalline silicon by focused ion beam, Sci. Rep. **8**, 11623 (2018).
[27] Y. Zhao, M. A. Belkin, and A. Alù, Twisted optical metamaterials for planarized ultrathin broadband circular polarizers, Nat. Commun. **3**, 870 (2012).
[28] C. F. Bohren and D. R. Huffman, *Absorption and Scattering of Light by Small Particles* (John Wiley & Sons, New York, 2008).
[29] M. V. Gorkunov, A. A. Antonov, and Y. S. Kivshar, Metasurfaces with Maximum Chirality Empowered by Bound States in the Continuum, Phys. Rev. Lett. **125**, 093903 (2020).
[30] A. Overvig, N. Yu, and A. Alu, Chiral quasi-bound states in the continuum, arXiv:2006.05484.
[31] I. Staude, A. E. Miroshnichenko, M. Decker, N. T. Fofang, S. Liu, E. Gonzales, J. Dominguez, T. S. Luk, D. N. Neshev, I. Brener, and Y. Kivshar, Tailoring directional scattering through magnetic and electric resonances in subwavelength silicon nanodisks, ACS Nano **7**, 7824 (2013).
[32] M. Kerker, D.-S. Wang, and C. L. Giles, Electromagnetic scattering by magnetic spheres, J. Opt. Soc. Am. **73**, 765 (1983).
[33] See Supplemental Material at http://link.aps.org/supplemental/10.1103/PhysRevLett.126.123201 for (i) spectral tuning and coupling of electric and magnetic modes, (ii) chiral metasurface characterization, (iii) Stimulated Raman Scattering modeling, (iv) Parameter space for nonreciprocal lasing, and (v) Lasing behavior.
[34] V. S. Asadchy, A. Díaz-Rubio, and S. A. Tretyakov, Bianisotropic metasurfaces: Physics and applications, Nanophotonics **7**, 1069 (2018).
[35] R. Alaee, M. Albooyeh, A. Rahimzadegan, M. S. Mirmoosa, Y. S. Kivshar, and C. Rockstuhl, All-dielectric reciprocal bianisotropic nanoparticles, Phys. Rev. B **92**, 245130 (2015).
[36] K. Koshelev, S. Lepeshov, M. Liu, A. Bogdanov, and Y. Kivshar, Asymmetric Metasurfaces with High-Q Resonances Governed by Bound States in the Continuum, Phys. Rev. Lett. **121**, 193903 (2018).
[37] S. Zhang, Y.-S. Park, J. Li, X. Lu, W. Zhang, and X. Zhang, Negative Refractive Index in Chiral Metamaterials, Phys. Rev. Lett. **102**, 023901 (2009).
[38] S. Zhang, F. Liu, T. Zentgraf, and J. Li, Interference-induced asymmetric transmission through a monolayer of anisotropic chiral metamolecules, Phys. Rev. A **88**, 023823 (2013).
[39] S. Yang, Z. Liu, S. Hu, A.-Z. Jin, H. Yang, S. Zhang, J. Li, and C. Gu, Spin-selective transmission in chiral folded metasurfaces, Nano Lett. **19**, 3432 (2019).
[40] S. Molesky, Z. Lin, A. Y. Piggott, W. Jin, J. Vucković, and A. W. Rodriguez, Inverse design in nanophotonics, Nat. Photonics **12**, 659 (2018).
[41] R. Pestourie, C. Pérez-Arancibia, Z. Lin, W. Shin, F. Capasso, and S. G. Johnson, Inverse design of large-area metasurfaces, Opt. Express **26**, 33732 (2018).
[42] D. Sell, J. Yang, S. Doshay, and J. A. Fan, Periodic dielectric metasurfaces with high-efficiency, multiwavelength functionalities, Adv. Opt. Mater. **5**, 1700645 (2017).
[43] Pumping a Raman-active crystal can also result in the absorption of a phonon, resulting in an anti-Stokes shifted sideband. However, the population of the anti-Stokes mode is significantly less than that of the Stokes mode at room temperature [19].
[44] M. Krause, Nonreciprocal light transmission in silicon by Raman-induced asymmetry of the permittivity tensor, J. Appl. Phys. **111**, 093107 (2012).
[45] M. Krause, H. Renner, and E. Brinkmeyer, Strong enhancement of Raman-induced nonreciprocity in silicon waveguides by alignment with the crystallographic axes, Appl. Phys. Lett. **95**, 261111 (2009).
[46] B. Jalali, V. Raghunathan, D. Dimitropoulos, and O. Boyraz, Raman-based silicon photonics, IEEE J. Sel. Topics Quantum Electron. **12**, 412 (2006).
[47] Y. Yang, W. Wang, A. Boulesbaa, I. I. Kravchenko, D. P. Briggs, A. Puretzky, D. Geohegan, and J. Valentine, Nonlinear Fano-resonant dielectric metasurfaces, Nano Lett. **15**, 7388 (2015).
[48] K. Rivoire, S. Buckley, and J. Vučković, Multiply resonant photonic crystal nanocavities for nonlinear frequency conversion, Opt. Express **19**, 22198 (2011).
[49] M. Minkov, D. Gerace, and S. Fan, Doubly resonant $\chi(2)$ nonlinear photonic crystal cavity based on a bound state in the continuum, Optica **6**, 1039 (2019).
[50] A. B. Khanikaev, S. Hossein Mousavi, W.-K. Tse, M. Kargarian, A. H. MacDonald, and G. Shvets, Photonic topological insulators, Nat. Mater. **12**, 233 (2013).
[51] L. Lu, J. D. Joannopoulos, and M. Soljačić, Topological photonics, Nat. Photonics **8**, 821 (2014).
[52] W.-J. Chen, S.-J. Jiang, X.-D. Chen, B. Zhu, L. Zhou, J.-W. Dong, and C. T. Chan, Experimental realization of photonic topological insulator in a uniaxial metacrystal waveguide, Nat. Commun. **5**, 5782 (2014).
[53] Y. Zhao, A. N. Askarpour, L. Sun, J. Shi, X. Li, and A. Alù, Chirality detection of enantiomers using twisted optical metamaterials, Nat. Commun. **8**, 14180 (2017).
[54] M. Solomon, J. Hu, M. Lawrence, A. García-Etxarri, and J. A. Dionne, Enantiospecific optical enhancement of chiral sensing and separation with dielectric metasurfaces, ACS Photonics **6**, 43 (2019).